Quasiperiodic waves at the onset of zero-Prandtl-number convection with rotation

Krishna Kumar,[1] Sanjay Chaudhuri,[2] and Alaka Das[1]
[1]*Physics and Applied Mathematics Unit, Indian Statistical Institute, 203, Barrackpore Trunk Road, Kolkata 700 108, India*
[2]*Statistics and Mathematics Unit, Indian Statistical Institute, 203, Barrackpore Trunk Road, Kolkata 700 108, India*
(Received 20 August 2001; published 24 January 2002)

We show the possibility of temporally quasiperiodic waves at the onset of thermal convection in a thin horizontal layer of slowly rotating zero-Prandtl-number Boussinesq fluid confined between stress-free conducting boundaries. Two independent frequencies emerge due to an interaction between straight rolls and waves along these rolls in the presence of Coriolis force, if the Taylor number is raised above a critical value. Constructing a dynamical system for the hydrodynamical problem, the competition between the interacting instabilities is analyzed. The forward bifurcation from the conductive state is self-tuned.

DOI: 10.1103/PhysRevE.65.026311 PACS number(s): 47.20.Ky, 47.27.Te

I. INTRODUCTION

The study of thermal convection in very low-Prandtl-number ($P=\nu/\kappa \ll 1$) fluids has been motivated by theoretical interests in the problems of astrophysics [1–4], geophysics [5], and turbulence [2,3], as well as its potential industrial applications in the problems of crystal growth [6,7] and heat transport in liquid metals [8,9]. In addition, both experimental and theoretical investigations of thermal convection at very low P have also contributed to our understanding of the mechanism of pattern-forming instabilities [10–16] in an extended dissipative system. The hydrodynamics, in Boussinesq approximation [17], is governed by two nonlinearities. The first, $\mathbf{v}\cdot\boldsymbol{\nabla}\mathbf{v}$, describes the self-interaction of the velocity field $\mathbf{v}$ and the second, $\mathbf{v}\cdot\boldsymbol{\nabla}\theta$, results from the interaction of the velocity field and the deviation θ from the conductive temperature field due to convection. These two nonlinearities are responsible for various instabilities and their saturation. At the onset of thermal convection in Boussinesq fluids confined between the conducting boundaries the straight [two-dimensional (2D)] rolls appear [17]. The nonlinear term $\mathbf{v}\cdot\boldsymbol{\nabla}\mathbf{v}$ does not saturate the temporally growing amplitude of the straight rolls just above the onset of convection in the presence of *stress-free* flat boundaries. It happens because $\mathbf{v}\cdot\boldsymbol{\nabla}\mathbf{v}$ yields zero for 2D rolls near the onset. The growing amplitude of 2D rolls is saturated by the nonlinearity $\mathbf{v}\cdot\boldsymbol{\nabla}\theta$. In the asymptotic limit of vanishing Prandtl number ($P\rightarrow 0$), the nonlinearity $\mathbf{v}\cdot\boldsymbol{\nabla}\theta$ in the heat equation is considered negligible [1] and, therefore, dropped. The set of 2D rolls with their amplitude growing exponentially in time, which is the exact solution of the linear system for $R>R_c$, then becomes an exact solution of the nonlinear hydrodynamical system in the close vicinity of the instability onset. Some of the 3D nonlinear solutions (e.g., squares and hexagons), which arise due to the nonlinear superposition of two or more sets of straight rolls, also fail to saturate the instability [18]. The limit has been, therefore, considered a complicated singular limit [19] for a long time. The nonsaturation of the instability is also known to occur in the case of inertial convection [20], where $\mathbf{v}\cdot\boldsymbol{\nabla}\mathbf{v}$ is compensated by a pressure gradient. A careful 3D direct numerical simulation (DNS) of Boussinesq equations in the limit of zero Prandtl number by Thual [14] showed saturation of the instability instead of indefinite temporal growth. He considered all possible modes for the vertical vorticity compatible with stress-free boundaries. When the growing amplitude of 2D rolls becomes large, wavy perturbations are spontaneously generated. These perturbations make rolls wavy along their axis. The exchange of energy between the waves and the straight rolls leads to the saturation of convective instability. The instability is *self tuned* [15] as they appear when the amplitude of the straight rolls grows above a large value with all bifurcation parameters (e.g., Rayleigh number R, Taylor number T, wave numbers k and q) kept fixed. The new bifurcation is *nonlocal* and *forward*.

We present, in this paper, a theoretical study of thermal convection in slowly rotating Boussinesq fluids of zero Prandtl number confined between conducting *stress-free* flat boundaries. The system shows interesting nonlinear dynamics. The linear stability shows that the *principle of exchange of stability* is valid for $T<27\pi^4/8$. The critical Rayleigh number R_0 and the critical wave number k_0 for the oscillatory convection are independent of Taylor number T in this limit. The nonlinear convection for small rotation rates is investigated by constructing a 12-mode dynamical system (see Appendix B) from the full hydrodynamical equations. We show that the convection sets in as temporal quasiperiodic waves for Taylor number T above a critical value T_c, although the *principle of exchange of stability* is valid at these Taylor numbers. To the best of our knowledge, the possibility of fluid flow varying quasiperiodically in time at the onset of the first instability has not been studied before for hydrodynamical systems. Earlier observations of quasiperiodic flows [21] in other fluid-dynamical systems were reported at the onset of secondary instability and not at the primary instability as is the case here. The generation of two independent frequencies is the result of an interaction between stationary instability and *self-tuned* waves in the presence of Coriolis force. For the values of Taylor number below T_c, the convection occurs in the form of 3D wavy rolls as is the case in the absence of rotation. The model also shows the possibility of a transition from one wavy solution to another through a narrow window of period-doubling instability. We have also verified the stability of these standing waves against traveling waves.

II. HYDRODYNAMICAL SYSTEM

We consider a thin layer of a Boussinesq fluid of infinite horizontal extension subjected to a uniform adverse temperature gradient β across the fluid layer, and a rigid body rotation with an angular velocity Ω about the vertical axis. The fluid is assumed to have uniform values of the kinematic viscosity ν and the thermal diffusivity κ. The basic state is the conductive state with no fluid motion in the rotating frame of reference. The convective flow, in the limit of zero Prandtl number, is then described by the following system of dimensionless hydrodynamic equations:

$$\partial_t(\nabla^2 v_3)=\nabla^4 v_3+R\nabla_H^2\theta-\sqrt{T}\partial_z\omega_3-\hat{\mathbf{e}}_3\cdot\boldsymbol{\nabla}\times[(\boldsymbol{\omega}\cdot\boldsymbol{\nabla})\mathbf{v}-(\mathbf{v}\cdot\boldsymbol{\nabla})\boldsymbol{\omega}], \tag{1}$$

$$\partial_t\omega_3=\nabla^2\omega_3+\sqrt{T}\partial_z v_3+[(\boldsymbol{\omega}\cdot\boldsymbol{\nabla})v_3-(\mathbf{v}\cdot\boldsymbol{\nabla})\omega_3] \tag{2}$$

$$\nabla^2\theta=-v_3, \tag{3}$$

where $\mathbf{v}(x,y,z,t)\equiv(v_1,v_2,v_3)$ is the velocity field, $\theta(x,y,z,t)$ the deviation in temperature field from steady conduction profile, and $\boldsymbol{\omega}\equiv(\omega_1,\omega_2,\omega_3)=\boldsymbol{\nabla}\times\mathbf{v}$ the vorticity field in the fluid. In the above, length scales are made dimensionless by the thickness d of the fluid layer, time by the viscous time scale d^2/ν, and the temperature field by $(\beta d)\nu/\kappa$. Rayleigh number $R=\alpha g\beta d^4/\nu\kappa$ and Taylor number $T=4\Omega^2 d^4/\nu^2$ are the two-dimensionless external parameters. The unit vector $\hat{\mathbf{e}}_3$ is directed vertically upward. We impose periodic boundary conditions in horizontal plane. This introduces two fundamental wave numbers k along x axis and q along y axis. The stress-free boundary conditions imply $\partial_z v_1=\partial_z v_2=v_3=0$ at $z=0,1$. Thermally conducting horizontal boundaries yield $\theta=0$ at $z=0,1$. The hydrodynamical Eqs. (1)–(3) are the same as those derived by Chandrasekhar [17]. We have made the fields also nondimensional, and have considered the case of zero P. We have also eliminated the pressure field from Navier-Stokes equations by taking the curl twice on the momentum equation and using the incompressibility condition $(\boldsymbol{\nabla}\cdot\mathbf{v}=0)$.

III. LINEAR STABILITY ANALYSIS

The linear stability analysis of the Rayleigh-Bénard convection with Coriolis force has been done by Chandrasekhar [17]. The critical Rayleigh number $R_c(T)$ and the critical wave number $k_c(T)$ for stationary convection are independent of the Prandtl number P. So, they remain unchanged in the limit of zero Prandtl number. They may be written as $R_c(T)=3[\pi^2+k_c^2(T)]^2$ and $k_c(T)=\pi\sqrt{l_1+l_2-1/2}$, where

$$l_{1,2}=\left(\frac{1}{4}\left\{\frac{1}{2}+\frac{T}{\pi^4}\pm\left[\left(\frac{1}{2}+\frac{T}{\pi^4}\right)^2-\frac{1}{4}\right]^{1/2}\right\}\right)^{1/3}.$$

In the absence of rotation, $k_c(T=0)$ and $R_c(T=0)$ take their standard values, which are $\pi/\sqrt{2}$ and $27\pi^4/4$, respectively. The critical Rayleigh number $R_0(T)$ and the critical wave number $k_0(T)$ for the oscillatory instability in rotating fluids depend, in general, on the Taylor number T as well as the Prandtl number P. In the limit of zero P, however, $k_0(T)=\pi/\sqrt{2}$ turns out to be independent of T. The critical Rayleigh number $R_0(T)=27\pi^4/2$ is also independent of T. The angular frequency ω_0, at the onset of oscillatory convection, is given by $\omega_0^2=\frac{2}{3}(T-27\pi^4/8)$. The angular frequency ω_0, is real, if the Taylor number T is above a fixed value $T_0=27\pi^4/8$. The *principle of exchange of stability* is, therefore, valid at the onset of thermal convection in rotating Boussinesq fluids of zero Prandtl number, if $T\leqslant T_0$. The oscillatory convection is possible for $T>T_0$. However, the oscillatory convection may occur as the primary instability *only if* $R_0<R_c(T)$. This happens for the values of Taylor number $T>T_*$ $(=544.700\,25\pm0.000\,05)$. The thermal convection in the limit of $P\to 0$ shows a bicritical point at $T=T_*$, when the stationary and the oscillatory solutions coexist.

IV. THE MODEL

The straight rolls, just above the onset of zero-Prandtl-number convection, are not the exact solution of the nonlinear hydrodynamic system with rotation as is the case in the absence of rotation. The only relevant nonlinearity $\mathbf{v}\cdot\boldsymbol{\nabla}\mathbf{v}$ does not yield zero. Nevertheless, 2D rolls are not saturated close to the instability onset. The saturation occurs only because of the nonlinear interaction of 2D rolls with 3D wavy perturbations, which make the rolls wavy along their axis. To understand the nonlinear behavior close to the onset of convection, we construct a consistent minimal-mode model using Galerkin technique [24]. We expand the vertical velocity v_3 and the vertical vorticity ω_3 in Fourier series compatible with the *stress-free* boundary conditions and conducting thermal boundary conditions. As the DNS, in absence of rotation, showed standing patterns [14] instead of traveling patterns, we expect similar behavior at least for small rotation rates. Therefore, we expand the fields with real Fourier coefficients. This lead to the following expansion for the vertical velocity and the vertical vorticity for a minimum-mode model.

$$\begin{aligned}v_3(x,y,z,t)=&W_{101}(t)\cos k_c x\sin\pi z\\&+W_{111}(t)\cos k_c x\cos qy\sin\pi z\\&+W_{\overline{111}}(t)\sin k_c x\sin qy\sin\pi z\\&+W_{012}(t)\cos qy\sin 2\pi z+\cdots\end{aligned} \tag{4}$$

$$\begin{aligned}\omega_3(x,y,z,t)=&\zeta_{101}(t)\cos k_c x\cos\pi z+\zeta_{010}(t)\cos qy\\&+\zeta_{111}(t)\cos k_c x\cos qy\cos\pi z\\&+\zeta_{\overline{111}}(t)\sin k_c x\sin qy\cos\pi z\\&+\zeta_{012}(t)\cos qy\cos 2\pi z+\zeta_{200}(t)\cos 2k_c x\\&+\zeta_{210}(t)\cos 2k_c x\cos qy\\&+\zeta_{\overline{210}}(t)\sin 2k_c x\sin qy+\cdots.\end{aligned} \tag{5}$$

The solenoidal character of the velocity and the vorticity fields yield their horizontal components (see, Appendix A).

The thermal fluctuation θ is slaved in this limit, and may be computed easily from Eq. (3).

The mode selection is quite systematic. As rotation couples the vertical velocity and the vertical vorticity linearly, we have selected the mode ζ_{101} for the vertical vorticity. The wavy mode ζ_{010} is the most dangerous at very low P, and, therefore, retained. All other modes appear through the nonlinear interaction of these vorticity modes with the critical velocity mode W_{101} and higher order velocity modes. As the vorticity field is crucial for the saturation of convection in the limit of vanishing Prandtl number, all relevant second harmonics are retained for the vertical vorticity. All second harmonics in the vertical velocity field, consistent with the selected vorticity modes, are also retained. Other higher order modes may be required as R and T are raised further. We have not considered other convective structures like squares [22] or hexagons, which are nonlinear superposition of straight rolls because they are unlikely to saturate the instability at the onset in $P\rightarrow 0$ limit. Küppers-Lortz instability [23], which occurs at relatively high T and involves two sets of straight rolls at an angle of 58°, is also not considered as we are concerned with saturation of the primary instability at low $T(<15)$. Wavy stripes are more likely to occur in this limit than structures involving straight rolls. We have retained essential modes to capture the nonlinear interaction between the stationary instability and the wavy instabilities just at the onset of convection. Projecting the hydrodynamic Eq. (1)–(3) on the selected modes [Eqs. (4) and (5)], we arrive at a 12-dimensional dynamical system (see, Appendix B). The model is expected to be good in the vicinity of the convective instability at low Taylor numbers.

V. RESULTS AND DISCUSSION

We now investigate the solutions of the dynamical system by performing numerical integration of the model using the standard fourth order Runge-Kutta scheme. We take a value for T, which fixes $k_c(T)$. We then choose a value for q. We have tried with different values of the wave number q of the perturbations and got qualitatively similar results for $0.2 \leqslant q/k_c \leqslant 0.65$. The model requires more modes outside this range of q. We present here all the results for $q/k_c(T) = 0.4$. Initial values for all the 12 modes are chosen randomly, and the integration is done for a fixed value of the Rayleigh number. We then repeat the procedure by increasing the value of R in small steps. We have also tried various initial conditions. The results of all the numerical integrations remain the same for identical values of all the relevant parameters. In the absence of rotation $(T=0)$, only six modes are excited. This model then reproduces the results of the model [15] of zero P convection without rotation. In the presence of rotation, all twelve modes are excited as they should in a consistent minimum-mode model. Small values of higher order modes (see Fig. 5) show the convergence properties of the model close to the onset of convection at the Taylor numbers considered.

Figure 1 gives the stability boundaries of various possible solutions, in the parameter space $R-T$, computed from the model dynamical system. The lowest line shows the dependence of the critical Rayleigh number R_c on Taylor number T for zero-Prandtl-number stationary convection in Boussinesq fluids. The overstability is ruled out for Taylor numbers considered here. As the Rayleigh number is raised above its critical value $R_c(T)$, the conductive state becomes unstable via stationary bifurcation. However, the temporal growth of the amplitude of the straight rolls does not stop if only 2D problem is considered. Figure 2 shows the mechanism of saturation. The total energy, spatially averaged over one convective cell, grows exponentially until the 3D waves are spontaneously generated. The generation of waves is shown by the spontaneous surge in v_2^2 (the bottom left in Fig. 2). The standing waves (SW1) so generated is periodic in time for $T<6.0$. This is similar to what happens in the absence of rotation in zero P Boussinesq fluids [15]. As Rayleigh number is increased slowly, the exchange of energy from 2D modes to 3D waves increases. Larger amplitude variation of the wavy modes is at the cost of the energy of 2D rolls. This is a well known feature in the case of oscillatory instability. The mechanism of saturation of the instability is quite different from that for the oscillatory instability [25].

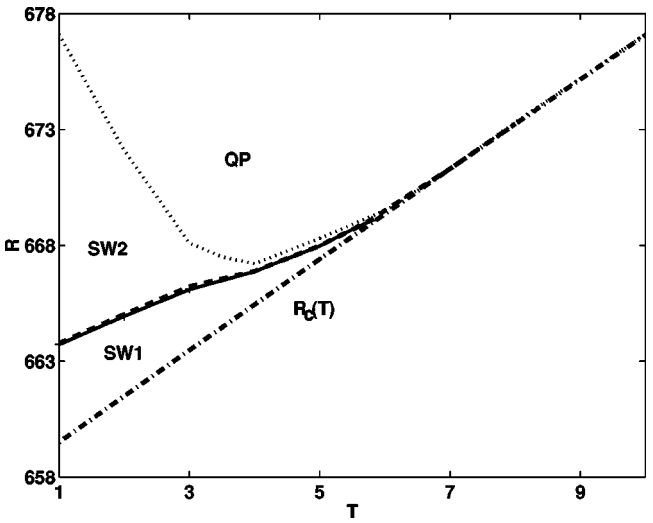

FIG. 1. Stability boundaries in the parameter space R-T just above the onset of convection. The conduction state is stable below the lowest line, which shows the critical value R_c of Rayleigh number as a function of Taylor number T for $q=0.4k_c$. The regions denoted by SW1 and SW2 show two regimes of wavy solutions separated by a thin region where period doubling is observed. Temporally quasiperiodic waves are predicted in the region marked QP.

As the Rayleigh number is increased further, the solution changes from one wavy solution to another through a narrow window of R showing period-doubling solutions (see the middle row of Fig. 3). The first wavy solution (SW1) has the modes W_{101} and ζ_{101} oscillating with nonzero mean, while the second wavy solution (SW2) has these modes oscillating with zero mean. In the later case the modes ζ_{010} and ζ_{210} oscillate with nonzero mean. The period of oscillation for the vorticity mode ζ_{010} is double that of the velocity mode W_{101} for both the waves. The mode W_{111} oscillates subharmonically for SW1 and harmonically for SW2 with respect to the mode W_{101}.

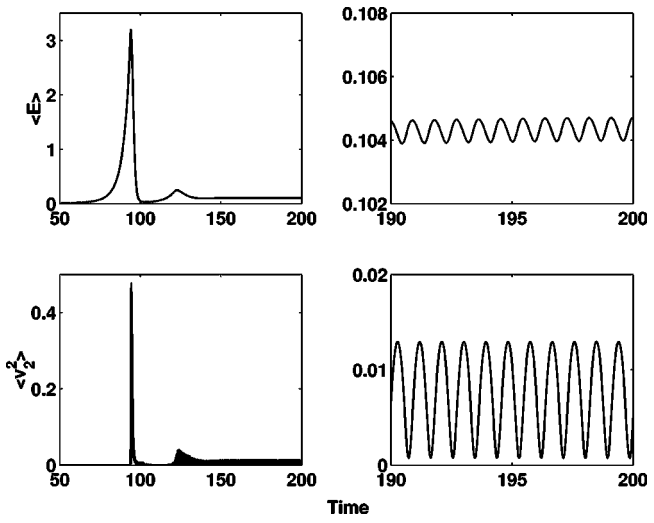

FIG. 2. The saturation mechanism for Taylor number $T<6.0$. The first column shows the temporal evolution of the spatially averaged total energy $\langle E\rangle$ (above) and the energy $\langle v_2^2\rangle$ (below) of waves along the roll axis for $T=2.0$ and $q=0.4k_c$. When the energy of straight rolls grows to a large but finite value, wavy perturbations are excited. The waves thus excited stop the further growth of 2D rolls. The interaction between the straight rolls and standing waves along the rolls leads to a limit cycle (second column).

As T is raised further, the rotation facilitates the exchange of more energy from the 2D roll mode W_{101} to the vorticity mode ζ_{101} through the linear coupling. We observe an interesting behavior for $T>6.0$ (see Fig. 1). The conduction state becomes unstable via stationary instability but the final state just above the onset is quasiperiodic waves in time. Figure 4

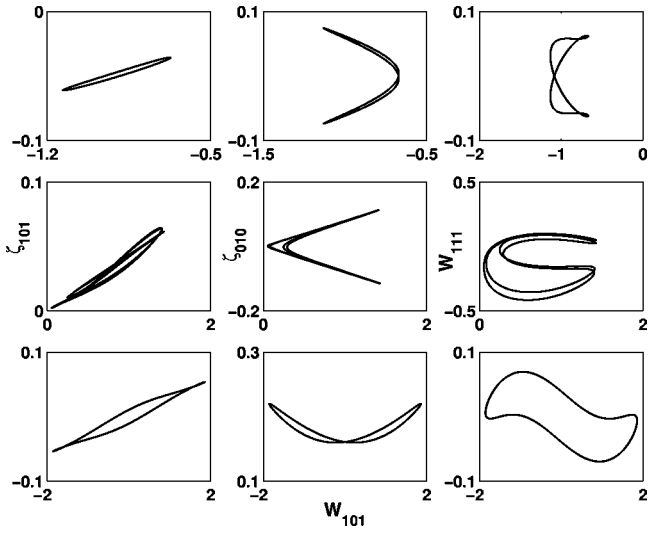

FIG. 3. Phase portrait for various values of the Rayleigh number R for $T=2.0$ and $q=0.4k_c$. The first, second, and third columns show the projections of the 12-dimensional phase space on $\zeta_{101}-W_{101}$, $\zeta_{010}-W_{101}$, and $W_{111}-W_{101}$ planes, respectively. The top row ($R=663.0$) and the bottom row ($R=668$) show two different wavy regimes SW1 and SW2, respectively, while the middle row ($R=664.95$) shows period doubling in a narrow regime between SW1 and SW2.

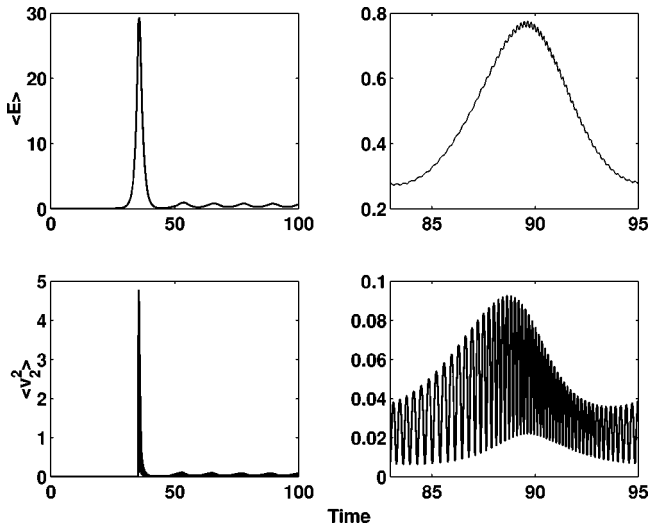

FIG. 4. The saturation mechanism for Taylor number $T>6.0$. When the energy $\langle E\rangle$ of straight rolls grows to a large but finite value, wavy perturbations $\langle v_2^2\rangle$ are excited ($T=10.0$ and $q=0.4k_c$). The interaction between the straight rolls and the standing waves along the roll-axis leads to two independent frequencies (second column) instead of one as is observed for $T<6.0$ (see Fig. 2).

shows the saturation mechanism of convection for $T>6.0$. When the total energy of 2D rolls becomes large, wavy perturbations are spontaneously excited as observed for $T<6.0$. However, the vertical vorticity due to rotation and the *self-tuned* 3D waves interact strongly. This interaction leads to the appearance of two independent frequencies at the onset of primary instability. Consequently, the amplitude of waves starts modulating. Figure 5 shows the variations of different modes with time. The amplitudes of all the modes

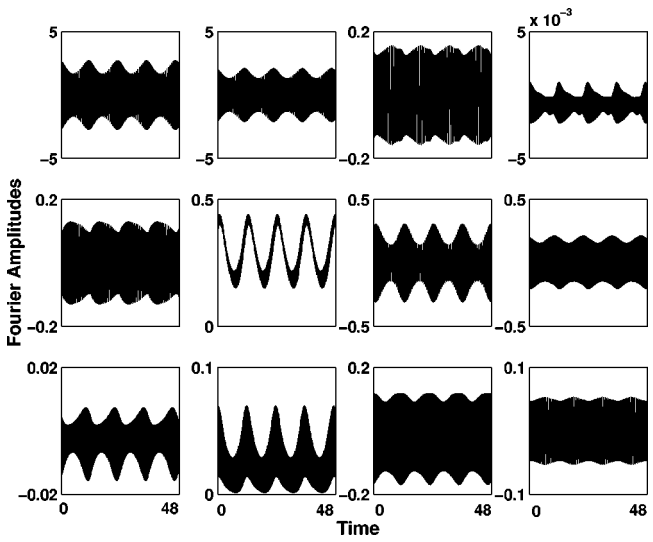

FIG. 5. Time variation of various modes for $T=10.0$, $q=0.4k_c$, and $R=678.0$ long after all transients have died out. The critical Rayleigh number $R_c(T=10.0)=677.076\,8$. Starting from left, the top row shows temporal variation of the modes W_{101}, $W_{\overline{111}}$, W_{111}, and W_{012}, respectively with time. The middle row shows the variation of ζ_{101}, ζ_{010}, ζ_{111}, and ζ_{200}. The bottom row shows the same for the modes ζ_{012}, ζ_{210}, $\zeta_{\overline{210}}$, and ζ_{110}.

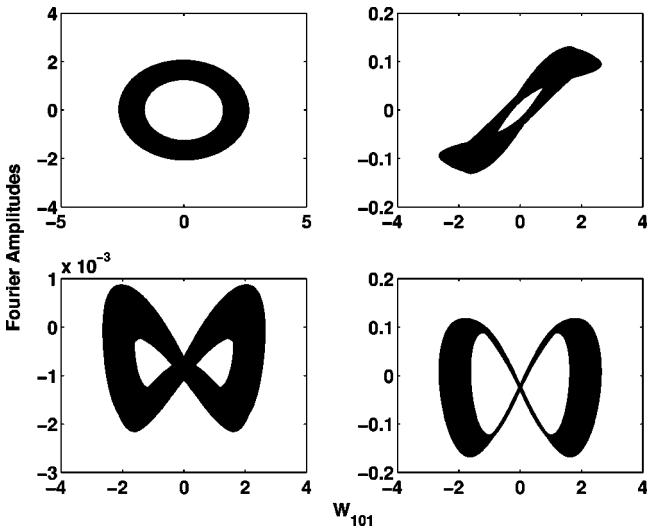

FIG. 6. Phase space portraits showing quasiperiodic motion for $T=10.0$, $q=0.4k_c$, and $R=677.08$. Starting clockwise from the left top, they show the projections of phase space in $W_{\overline{111}}-W_{101}$, $\zeta_{101}-W_{101}$, $\zeta_{\overline{210}}-W_{101}$, and $W_{012}-W_{101}$ planes, respectively.

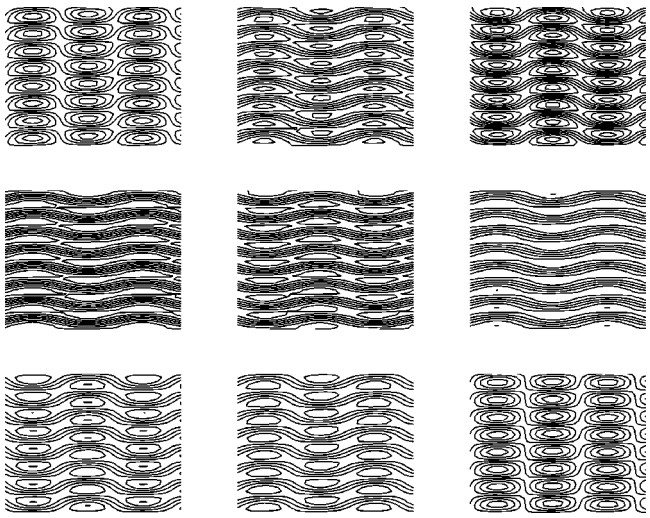

FIG. 7. Contour plots ($T=7.0$, $q=0.4k_c$, and $R=671.30$ at $z=0.25$). Various textures of the pattern are shown over a period of faster time scale t_0 at equal time intervals of $t_0/8$. The sequence of time evolution of the pattern texture is shown from left to right in each row starting from the top row.

begin modulating at the same frequency. The Fourier transforms of these modes show two independent frequencies. The frequency of amplitude modulation is much smaller compared to that of waves. The sharp decrease of the amplitudes of higher order modes (see Fig. 5) confirms the fast convergence of the expansion. The model, therefore, represents accurately the scenario close to the instability onset. Figure 6 shows the projections of phase space trajectories in various phase planes. It clearly describes the quasiperiodic nature of the convective flow. The trajectories are confined in a 12-dimensional torus in the phase space. The quasiperiodic behavior originates due to the nonlinear interaction among the 2D velocity mode W_{101}, the 2D vorticity mode ζ_{101} excited by rotation, and the wavy mode ζ_{010}. Figure 7 reveals some interesting details of the time dependence of convective patterns. The complex textures of the quasiperiodic patterns are shown for a period of the wavy motion, which is much faster than the amplitude modulation. Two halves of a period of the wavy motion are quite asymmetric. The textures of the pattern at different times are never the same due to quasiperiodicity.

We now consider the stability of the standing waves against possible traveling waves along the roll axis. This is facilitated by adding a mode $\zeta_{0\overline{10}}(t)\sin qy$ and all higher order modes arising due to the nonlinear coupling between this mode and the velocity modes. This led to six more modes for the vorticity and three higher modes for the vertical velocity. The resulting model, consisting of 21 modes, reduces to the 12-mode model on integration for Taylor number considered here. Depending upon the initial conditions either ζ_{010} or $\zeta_{0\overline{10}}$ is excited at the primary instability. This shows that the standing waves are preferred at the onset. This may be connected to the fact that the limit of zero P removes the nonlinearity $\mathbf{v}\cdot\boldsymbol{\nabla}\theta$.

We have presented in this paper a simple dynamical system, derived from the full hydrodynamical equations, which describes the phenomenon of thermal convection in slowly rotating Boussinesq fluids of zero Prandtl number just above the onset. For values of Taylor number below T_c, one wavy solution bifurcates to another via a narrow window of period-doubling instability as the Rayleigh number R is increased. For $T>T_c$, quasiperiodic waves are observed at the onset of thermal convection. This is possible in spite of the fact that the *principle of exchange of stability* is valid according to the linearized hydrodynamical system. The instability is an example of *self-tuned* forward bifurcation purely due to nonlinear effects. The conductive state bifurcates directly to the quasiperiodic waves at the primary instability. The model presented would be also useful to study an interesting possibility of transition from a state of rest to quasiperiodic chaos [21,26] close to the primary instability.

ACKNOWLEDGMENT

This work is supported by grants from DST, Government of India under the project, ''Pattern-forming instability and interface waves.''

APPENDIX A: HORIZONTAL VELOCITY AND VORTICITY FIELDS

The horizontal components of the velocity and the vorticity fields are given by

$$v_1(x,y,z,t)=-\frac{\pi}{k_c}W_{101}(t)\sin k_c x\cos\pi z-\frac{1}{q}\zeta_{010}(t)\sin qy$$

$$-\frac{1}{q}\zeta_{012}(t)\sin qy\cos 2\pi z$$

$$-\frac{q}{4k_c^2+q^2}\zeta_{210}(t)\cos 2k_c x\sin qy$$

$$+\frac{q}{4k_c^2+q^2}\zeta_{\overline{210}}(t)\sin 2k_cx\cos qy$$
$$+\left[\frac{\pi k_c}{k_c^2+q^2}W_{\overline{111}}(t)\right.$$
$$\left.-\frac{q}{k_c^2+q^2}\zeta_{111}(t)\right]\cos k_cx\sin qy\cos\pi z$$
$$-\left[\frac{\pi k_c}{k_c^2+q^2}W_{111}(t)\right.$$
$$\left.-\frac{q}{k_c^2+q^2}\zeta_{\overline{111}}(t)\right]\sin k_cx\cos qy\cos\pi z, \tag{A1}$$

$$v_2(x,y,z,t)=\frac{1}{k_c}\zeta_{101}(t)\sin k_cx\cos\pi z+\frac{1}{2k_c}\zeta_{200}(t)\sin 2k_cx$$
$$-\frac{2\pi}{q}W_{012}(t)\sin qy\cos 2\pi z$$
$$-\frac{2k_c}{4k_c^2+q^2}\zeta_{\overline{210}}(t)\cos 2k_cx\sin qy$$
$$+\frac{2k_c}{4k_c^2+q^2}\zeta_{210}(t)\sin 2k_cx\cos qy$$
$$-\left[\frac{\pi q}{k_c^2+q^2}W_{111}(t)\right.$$
$$\left.+\frac{k_c}{k_c^2+q^2}\zeta_{\overline{111}}(t)\right]\cos k_cx\sin qy\cos\pi z$$
$$+\left[\frac{\pi q}{k_c^2+q^2}W_{\overline{111}}(t)\right.$$
$$\left.+\frac{k_c}{k_c^2+q^2}\zeta_{111}(t)\right]\sin k_cx\cos qy\cos\pi z, \tag{A2}$$

$$\omega_1(x,y,z,t)=\frac{\pi}{k_c}\zeta_{101}(t)\sin k_cx\sin\pi z$$
$$-\frac{(4\pi^2+q^2)}{q}W_{012}(t)\sin qy\sin 2\pi z$$
$$-\left[\frac{q(\pi^2+k_c^2+q^2)}{k_c^2+q^2}W_{111}(t)\right.$$
$$\left.+\frac{\pi k_c}{k_c^2+q^2}\zeta_{\overline{111}}(t)\right]\cos k_cx\sin qy\sin\pi z$$
$$+\left[\frac{q(\pi^2+k_c^2+q^2)}{k_c^2+q^2}W_{\overline{111}}(t)\right.$$
$$\left.+\frac{\pi k_c}{k_c^2+q^2}\zeta_{111}(t)\right]\sin k_cx\cos qy\sin\pi z, \tag{A3}$$

$$\omega_2(x,y,z,t)=\frac{\pi^2+k_c^2}{k_c}W_{101}(t)\sin k_cx\sin\pi z$$
$$+\frac{2\pi}{q}\zeta_{012}(t)\sin qy\sin 2\pi z$$
$$-\left[\frac{k_c(\pi^2+k_c^2+q^2)}{k_c^2+q^2}W_{\overline{111}}(t)\right.$$
$$\left.-\frac{\pi q}{k_c^2+q^2}\zeta_{111}(t)\right]\cos k_cx\sin qy\sin\pi z$$
$$+\left[\frac{k_c(\pi^2+k_c^2+q^2)}{k_c^2+q^2}W_{111}(t)\right.$$
$$\left.-\frac{\pi q}{k_c^2+q^2}\zeta_{\overline{111}}(t)\right]\sin k_cx\cos qy\sin\pi z. \tag{A4}$$

APPENDIX B: THE DYNAMICAL SYSTEM

The 12-mode dynamical system reads

$$\dot a_1=\tau^2\left(Rk_c^2-\frac{1}{r^3}\right)a_1-\pi^2\tau\sqrt{T}b_1$$
$$+[(\pi^2-3k_c^2-2q^2)\tau\beta]a_3a_4$$
$$-2\alpha^{-1}[\beta-(\pi^2-k_c^2)\tau\beta']a_2b_2$$
$$-2\alpha^{-1}f_1a_2b_5-\delta f_1(a_3b_7+10a_2b_6)$$
$$-[4\alpha\beta\tau(\pi^2-k_c^2)]a_4b_8$$
$$+2\pi^2\beta\tau(b_2+b_5+10\alpha\delta b_6)b_3$$
$$-4\pi^2\alpha\beta\delta\tau b_7b_8, \tag{B1}$$

$$\dot a_2=\gamma^2\left(R(k_c^2+q^2)-\frac{1}{\gamma^3}\right)a_3+2\gamma\pi^2\sqrt{T}b_8+\alpha^{-1}a_1b_2$$
$$+f_2a_1(\alpha^{-1}b_5+5\delta b_6)+f_3a_3b_4+f_4a_4b_1$$
$$-2\pi^2\alpha\delta\gamma b_1b_7+4\pi^2\beta'\gamma b_4b_8, \tag{B2}$$

$$\dot a_3=\gamma^2\left(R(k_c^2+q^2)-\frac{1}{\gamma^3}\right)a_3+2\gamma\pi^2\sqrt{T}b_3-f_5a_1a_4$$
$$-\frac{2\delta\gamma}{\tau}a_1b_7-4f_3a_2b_4-4\pi^2\gamma b_1(b_2+b_5)$$
$$-20\pi^2\alpha\delta\gamma b_1b_6-\pi^2\beta'\gamma b_3b_4, \tag{B3}$$

$$\dot a_4=\eta^2\left(Rq^2-\frac{1}{\eta^3}\right)a_4+2\pi^2\eta\sqrt{T}b_5+f_6a_1a_3+f_7a_1b_8$$
$$+f_8a_2b_1-\pi^2\beta'\eta b_1b_3, \tag{B4}$$

$$\dot{b}_1=-\frac{1}{\tau}b_1+\sqrt{T}a_1+a_1b_4+\frac{2\alpha\beta}{\pi^2\gamma}a_2a_4-2\beta a_2b_7+\beta a_3(b_2+b_5-5b_6)+2\beta a_4b_3+2\alpha^{-1}\beta(4b_2+b_5)\times b_8+6\beta\delta(b_3b_7+10b_6b_8), \tag{B5}$$

$$\dot{b}_2=-q^2b_2-\frac{\alpha\beta'}{2}(a_1a_2+2b_1b_8)-\frac{\beta'}{4}(2a_1b_3-a_3b_1)-\alpha^2\delta b_4b_7, \tag{B6}$$

$$\dot{b}_3=-\frac{1}{\gamma}b_3-\frac{\sqrt{T}}{2}a_3-a_1(b_2+3b_5-5b_6)+\frac{\beta'-\beta}{2}a_3b_4+\tfrac{3}{2}a_4b_1+f_9b_1b_7+\alpha(3\beta-\beta')b_4b_8, \tag{B7}$$

$$\dot{b}_4=-4k_c^2b_4-\tfrac{3}{4}a_1b_1-2\beta(2a_2b_8-a_3b_3)+\frac{16\delta}{\alpha^2}b_2b_7, \tag{B8}$$

$$\dot{b}_5=-\frac{1}{\eta}b_5+2\sqrt{T}a_4+\frac{\alpha\beta'}{4}(a_1a_2+b_1b_3)+\frac{\beta'}{4}(a_1b_3+2a_3b_1), \tag{B9}$$

$$\dot{b}_6=-(4k_c^2+q^2)b_6+\frac{\alpha\beta'}{20}(a_1a_2+2b_1b_8)-\frac{4\beta+3\beta'}{40}(a_1b_3+a_3b_1), \tag{B10}$$

$$\dot{b}_7=-(4k_c^2+q^2)b_7+\frac{\alpha\beta'}{8}(a_1a_3+2b_1b_3)-\frac{4\beta+3\beta'}{4}(2a_1b_8-a_2b_1)-\frac{4\alpha'-\alpha}{2}b_2b_4, \tag{B11}$$

$$\dot{b}_8=-\frac{1}{\gamma}b_8-\frac{\sqrt{T}}{2}a_2+\frac{1}{2}a_1b_7+\frac{\beta-\beta'}{2}a_2b_4-\frac{\alpha+\alpha^{-1}}{2}b_1b_2+\frac{\alpha-\alpha^{-1}}{2}b_1b_5-\frac{5(3+\alpha^2)\delta}{2}b_1b_6+\frac{\alpha(3\beta-\beta')}{4}b_3b_4, \tag{B12}$$

where the temporal variables a_1's and b_1's are defined as

$$(a_1,a_3)=-\frac{\pi}{\sqrt{2}}(W_{101},-W_{111}),\quad (a_2,a_4)=-\frac{\pi}{2\sqrt{2}}\left(W_{\overline{111}},-\frac{1}{\sqrt{2}}W_{012}\right),\quad b_1=-\frac{1}{\sqrt{2}}\zeta_{101},$$

$$(b_2,b_4)=-\tfrac{1}{2}(\zeta_{010},\zeta_{200}),\quad (b_3,b_8)=-\frac{1}{2\sqrt{2}}(\zeta_{111},-\tfrac{1}{2}\zeta_{\overline{111}}),\quad b_5=-\tfrac{1}{4}\zeta_{012},$$

$$(b_6,b_7)=-\tfrac{1}{4}(\tfrac{1}{5}\zeta_{210},-\zeta_{\overline{210}}).$$

The coefficients in the above dynamical system are

$$\tau=(\pi^2+k_c^2)^{-1},\quad \alpha=q/k_c,\quad \beta=k_c^2/(k_c^2+q^2),$$

$$\beta'=\alpha^2\beta,\quad \delta=k_cq/(4k_c^2+q^2),\quad \gamma=(\pi^2+k_c^2+q^2)^{-1},$$

$$\eta=(4\pi^2+q^2)^{-1},\quad f_1=[(3\pi^2-k_c^2)\beta+(\pi^2-k_c^2)\beta']\tau,$$

$$f_2=\gamma(3\pi^2-k_c^2-q^2),\quad f_3=\alpha(\beta'-\beta f_2)/4,$$

$$f_4=\alpha\gamma(3\pi^2+k_c^2+q^2),\quad f_5=2\pi\gamma(5\pi^2+k_c^2+q^2),$$

$$f_6=\beta'\eta(3\pi^2+2k_c^2+2q^2)/8,\quad f_7=\alpha\beta\eta(3\pi^2-q^2)/2,$$

$$f_8=\alpha\eta(4\pi^2\beta-q^2)/4,\quad f_9=(3+\alpha^2)\delta.$$

[1] E. A. Spiegel, J. Geophys. Res. **67**, 3062 (1970).
[2] R. H. Kraichnan and E. A. Spiegel, Phys. Fluids **5**, 583 (1962).
[3] J. R. Herring, Woods Hole Oceanography Institute Technical Report No. WHOI-70-01, 1970.
[4] P. L. Sulem, C. Sulem, and O. Thual, Prog. Astronaut. Aeronaut. **100**, 125 (1985).
[5] F. H. Busse, *Fundamentals of Thermal Convection, Mantle Convection, Plate Tectonics, and Global Dynamics*, edited by W. R. Peltier (Gordon and Breach, New York, 1989), pp. 23–95.
[6] Y.-S. Lee and Ch-H. Chun, J. Cryst. Growth **180**, 477 (1997); **197**, 297 (1999).
[7] J. N. Koster, T. Seidel, and R. Derebail, J. Fluid Mech. **343**, 29 (1997); J. N. Koster, Eur. J. Mech. B/Fluids **16**, 447 (1997).
[8] A. Chiffaudel, S. Fauve, and B. Perrin, Europhys. Lett. **4**, 555 (1987).
[9] J. Friedrich, Y.-S. Lee, B. Fischer, C. Kupler, D. Vizman, and G. Müller, Phys. Fluids **11**, 853 (1999).
[10] F. H. Busse and R. M. Clever, J. Fluid Mech. **102**, 75 (1981).
[11] V. Croquette, Contemp. Phys. **30**, 113 (1989); **30**, 153 (1989).
[12] R. M. Clever and F. H. Busse, Phys. Fluids A **2**, 334 (1990).
[13] G. Ahlers, Phys. Rev. Lett. **71**, 2026 (1993); Y. C. Hu, R. Ecke, and G. Ahlers, *ibid.* **72**, 2191 (1994); J. Liu and G. Ahlers, *ibid.* **77**, 3126 (1996); G. Ahlers and K. M. S. Bajaj, in *Proceedings of IMA Workshop on Pattern Formation in Continuous and Coupled System*, edited by M. Golubitsky, D. Luss, and S. Strogatz (Springer, New York, 1999).
[14] O. Thual, J. Fluid Mech. **240**, 229 (1992).
[15] K. Kumar, S. Fauve, and O. Thual, J. Phys. II **6**, 945 (1996).
[16] P. Pal and K. Kumar, e-print nlin. PS/0103056.
[17] S. Chandrasekhar, *Hydrodynamic and Hydromagnetic Stability* (Oxford University Press, New York, 1961).

[18] K. Kumar, Woods Hole Oceanography Institute Technical Report No. WHOI-90-01, 1990.
[19] M. C. Cross and P. C. Hohenberg, Rev. Mod. Phys. **65**, 851 (1993).
[20] M. R. Proctor, J. Fluid Mech. **82**, 97 (1977).
[21] G. Ahlers, Phys. Rev. Lett. **33**, 1185 (1974); J. P. Gollub and H. Swinney, *ibid.* **35**, 927 (1975); M. Dubois and P. Berge, J. Phys. (France) Lett. **42**, 167 (1981).
[22] G. Veronis, J. Fluid Mech. **5**, 401 (1957).
[23] G. Küppers and D. Lortz, J. Fluid Mech. **35**, 609 (1969); R. J. Donnelly, Phys. Rev. Lett. **57**, 2524 (1986); Y. Hu, W. Pesch, G. Ahlers, and R. E. Ecke, Phys. Rev. E **58**, 5821 (1998).
[24] E. N. Lorenz, J. Atmos. Sci. **20**, 130 (1963); J. B. McLaughlin and P. C. Martin, Phys. Rev. A **12**, 186 (1975).
[25] F. H. Busse, J. Fluid Mech. **52**, 97 (1972); S. Fauve, E. W. Bolton, and M. E. Brachet, Physica D **29**, 202 (1987).
[26] D. Ruelle and F. Takens, Commun. Math. Phys. **20**, 167 (1971); **23**, 344 (1971).